

Hydration Mimicry by Membrane Ion Channels

Mangesh I. Chaudhari,¹ Juan M. Vanegas,¹ L. R. Pratt,² Ajay Muralidharan,² and Susan B. Rempe¹

¹Computational Biology and Biophysics Department, Sandia National Laboratories, Albuquerque, NM, 87185

²Department of Chemical and Biomolecular Engineering, Tulane University, New Orleans, LA, 70118

Xxxx. Xxx. Xxx. Xxx. YYYY. AA:1–29

[https://doi.org/10.1146/\(\(please add article doi\)\)](https://doi.org/10.1146/((please add article doi)))

Copyright © YYYY by Annual Reviews.
All rights reserved

Keywords

biomolecular hydration mimicry, membrane ion channels, hydration of metal ions, hydration free energy, hydration structure, quasi-chemical theory, density functional theory, statistical thermodynamic theory, KcsA, MgtE, Ca_vAb

Abstract

Ions transiting biomembranes might pass readily from water through ion-specific membrane proteins if those protein channels provide environments similar to the aqueous solution hydration environment. Indeed, bulk aqueous solution is an important reference condition for the ion permeation process. Assessment of this hydration mimicry view depends on understanding the hydration structure and free energies of metal ions in water to provide a comparison for the membrane channel environment. To refine these considerations, we review local hydration structures of ions in bulk water, and the molecular quasi-chemical theory that provides hydration free energies. In that process, we note some current views of ion-binding to membrane channels, and suggest new physical chemical calculations and experiments that might further clarify the hydration mimicry view.

Contents

1. BACKGROUND	2
1.1. Ions in Water	3
1.2. Ions in Protein Binding Sites	6
1.3. Specific Ions and Proteins for Hydration Mimicry Analysis	7
2. QUASI-CHEMICAL THEORY	9
2.1. Inner-shell Clusters	9
2.2. Potential of the Phase	11
2.3. QCT and Protein Binding Sites.....	12
3. ION HYDRATION STRUCTURE.....	13
4. ION HYDRATION FREE ENERGY	15
5. LOCAL STRUCTURE COMPARISON	16
6. CONCLUSIONS	20
7. ACKNOWLEDGMENT	21

1. BACKGROUND

Cells control salt concentration differences across boundary membranes by transporting ions selectively (1). Selective ion transport plays an important role in numerous physiological functions, including electrical signaling and cell volume control. Toward that end, proteins — either channels or transporters — provide pathways for ions to permeate. Blocking such pathways can have detrimental or beneficial effects. In beneficial cases, drugs that block specific channels hold promise for treating neurological disorders, autoimmune diseases, and cancers (2, 3, 4). Peptide toxins from several poisonous animals provide examples of the detrimental possibilities (5, 6). Indeed, simple divalent metal ions can be potent channel blockers, and both monovalent and divalent ions permeate selectively. In addition to important roles in health, cellular mechanisms of ion transport also can guide materials science by inspiring (7, 8), or being integrated into (9, 10), synthetic membranes for efficient power generation, water purification, mineral recovery, and separation of small molecules from mixtures (11).

According to a concept called “hydration mimicry,” ions might pass easily from water through protein channels when pore-lining amino acid residues arrange a local environment that mimics the local ion hydration environment (12, 13, 14, 15). Here, “local” structure refers to atoms that interact with an ion, making direct contacts. That local structural similarity may lead to a free energy for ion binding that approximately equals the free energy for ion hydration in bulk liquid water, with moderate barriers leading to rapid ion permeation (Figure 1).

Similarly, non-native ions may encounter large free energy barriers, leading to rejection from the protein pore if a binding site offers a poor hydration mimic (Figure 1). Alternatively, a non-native ion may be trapped by binding too strongly to a channel (Figure 1), and block passage of a native permeant ion (16, 17, 18, 19, 20).

Primitive concepts for design of biomimetic transport (21, 22) can begin with focus on the direct contacts of an ion in transit, and the consequences for the binding free energies. Contacts should be chemically competent for binding that is satisfactory, but not too strong (23). Those binding contacts should be available, and be flexible enough to accommodate ions in satisfactory binding geometries. Binding geometries may be characterized by prop-

erties like the number of contacts, or coordination number, and the distance between an ion and its contacts, or cavity size. Binding geometries also may be constrained by properties of the binding sites like covalent bonds, or by interactions with the proximal environment. Longer-range interactions, electrostatic and dispersion, are also essential, but perhaps not decisive in comparing ions with the same charge and similar sizes. Few approaches can treat all of these features. Fortunately, recent statistical thermodynamic theory — quasi-chemical theory (QCT) — offers a descriptive tool that facilitates analysis of those primitive structural concepts and their effect on ion binding free energies. QCT is a feature of the presentation that follows.

It is tempting to go further with refined hydration mimicry concepts, say, by noting interesting higher-resolution details of ion-protein binding configurations. But such comparisons have been limited by lack of the corresponding higher-resolution characterization of the binding of relevant ions to the bulk solution, which defines endpoints of ion transfer. Securing the natural bulk ion hydration details has been a challenge (24, 25, 26, 27). Here, we collect and discuss those important results, which have been obtained in recent work.

Theoretical studies (28, 29, 30) that assess the structure-free energy relationship between ion binding to a protein, relative to binding in water, are rarer than direct numerical simulation of such systems despite an abundance of high-resolution cryo-electron microscopy and crystal structures for channels and transporters. Here, we analyze the hydration mimicry concept by comparing local structure exhibited by molecular simulations of ion hydration and crystal structures of ion binding sites in channels and transporters. We also connect local hydration structure with the free energy of ion binding to water. Our results emphasize the importance of coordination number, and of neighborhood analyses of molecular simulations, to characterize local ion hydration structure, thus permitting comparison with experimental data on local structure for ions in channel and transporter binding sites. Neighborhood analyses also enhance the utility of the quasi-chemical free energy theory (QCT) for testing the hydration mimicry idea. Altogether, our results highlight unexpected relationships between local solvent structure and transfer free energies for ion permeation, rejection, and trapping that support an expanded view of hydration mimicry.

1.1. Ions in Water

Water is the reference environment for ion transport across cellular membranes. Transport takes ions from one aqueous solution to another, and may bring water molecules along as well (1, 31, 32, 33, 34). Since protein channels and transporters catalyze ion transport across cellular membranes, transport reflects a balance between ion-water interactions (23) and ion-protein interactions (35). Water molecules and functional groups from proteins may interact directly with transiting ions (13, 18, 36, 37, 38), providing ligands and defining the local ion solvation structure.

In assessing whether channel and transporter proteins form binding sites that mimic the local hydration structures of ions that readily permeate, a one ingredient is the hydration properties of ions in the reference environment of bulk liquid water. Ions and water form preferred coordination structures and those preferred structures may not be attainable in protein environments (28, 39, 40, 41).

Studies of ion hydration structure and hydration free energy benefit from combining experimental and theoretical approaches (26, 42, 43, 44). In the case of hydration structure, experiments can provide information about average water structure. Molecular simula-

Bulk aqueous reference: Bulk hydration studies provide information about the reference environment, *i.e.*, the end points that bracket a transit path for ions across membranes.

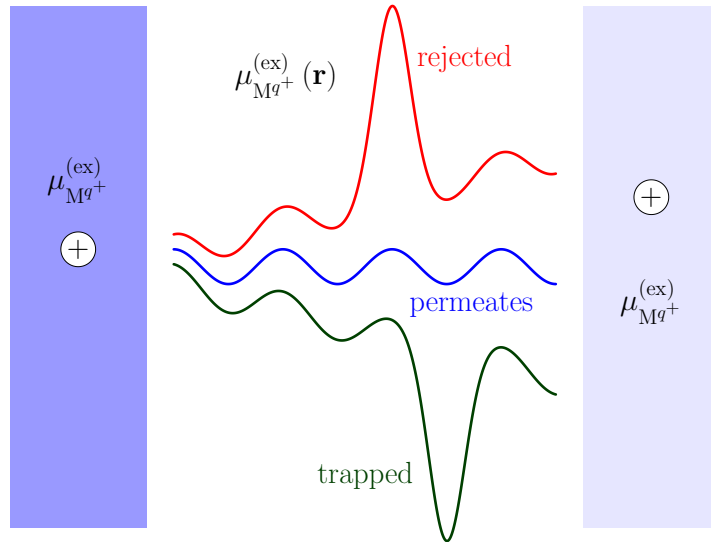


Figure 1

Do ion channels mimic the aqueous hydration of ions that readily permeate? Hypothetical molecular-scale variation of the free energies of ion binding, $\mu_{M^{q+}}^{(ex)}(\mathbf{r})$, illustrate rejected, permeating, or trapped cases.

tions, verified against experimental data, can resolve average structure into contributions from individual water molecules. That resolution identifies local hydration structure, the information sought here. The structural predictions can be scrutinized further by using local structures to build predictions of ion hydration free energies, also tested for consistency with experimental data in gas and liquid phases. In this way, local ion hydration structure is reliably connected to ion hydration free energy, providing insights about the mechanism of ion hydration. Further description of this overall approach follows below.

1.1.1. Hydration structure. Experiments that probe ion hydration structure include neutron and X-ray diffraction techniques that report differential scattering cross-sections leading to partial structure factors (43). An alternative technique, extended X-ray absorption fine structure (EXAFS) spectroscopy, also provides data related to partial structure factors (45, 46, 47). These factors can be determined with good accuracy, and yield pair-wise radial distribution functions (RDF) between ions and water oxygens. The RDF establishes information that characterizes the structure of solvent around ions of interest. For example, integrating the RDF through an inner-shell yields hydration numbers of ions.

In practice, significant challenges of good spectral resolution and momentum cutoffs (for diffraction work) are encountered in obtaining accurate experimental hydration numbers. Nevertheless, recent developments in both data acquisition and analysis, motivated in part by molecular simulation studies based on *ab initio* approaches and QCT (24), have significantly advanced experimental results (43). Even with accurate hydration numbers determined from experiment, information about local hydration structure may still be lacking. *Ab initio* molecular dynamics (AIMD) simulations can further differentiate local structural features, e.g. disposition of the closest water molecule, from the aggregated hydration

structure defined conventionally by the RDFs.

As with experiments, AIMD simulation results are challenged by demands of realistic access to suitable ranges of space and time (48). Nevertheless, recent developments in both algorithms and computer power have extended that ability, leading to improved information on ion hydration structures (49, 50, 51, 52, 53, 54, 55, 56, 57). Our presentation here highlights the correspondence between ion hydration structure illuminated by AIMD simulations with available experiment.

To resolve local structure, simulation calculations can provide natural neighborhood analyses of ion hydration structures, providing information not readily obtained from experiments. Those analyses distinguish the water molecules directly contacting an ion from those ligands that split time between ion contact and more distant solvent environments. Distinguishing ‘non-split shell’ and ‘split-shell’ water molecules helps in assessing the hydration mimicry idea.

While not broadly implemented so far (30, 44, 58, 59, 60), neighborhood analyses should be more widely used due to clear conceptual connection to solvation free energy on the basis of molecular quasi-chemical theory. At the same time, solvation free energies computed by QCT test local structural predictions, and facilitate the testing of concepts of solvation mechanism based on coordination numbers and other primitive concepts described above for design of biomimetic transport.

Neighborhood:

Neighborhood analyses describe the structures of the ligands closest to an ion, and can reveal ‘split-shell’ coordination structures.

1.1.2. Hydration free energy. Predictions of ion hydration free energies from molecular simulations face numerous challenges. One significant challenge arises because ion-water interactions are complicated beyond commonly used molecule-pair interaction models. Those complications reflect solvent polarizability and multi-molecule interactions generally, which affect interactions in the local solvation environment (61, 62). That complexity calls again for an approach that takes into account electronic degrees of freedom (48).

Another challenge arises with calculations of ion hydration free energies with QCT based on treating inner-shell clusters together with the initial assumption of small displacements (thus harmonic motions) of water molecules neighboring an ion. Recent work has refined this issue, but it deserves further development (63).

Free energy contributions from hydration of isolated clusters are computed separately in QCT. Properties of those clusters are accessible from experiments, such as high pressure mass spectrometry (64). The latter experiments determine the free energies of equilibrium cluster association reactions in gas phase (65), and also can be compared directly with, or even incorporated into, QCT analyses.

Recent work (44, 63, 66) provided examples of coupling between experiment and theory to predict ion hydration free energies, incorporating gas phase ion clustering free energies into QCT for halide ions. That work accounted for anharmonic vibrational motions observed spectroscopically in clusters with several coordinating waters (67). Further, density functionals used in AIMD simulations were selected to reproduce peak positions in experimentally determined radial distribution functions (RDF). Hydration free energy predictions yielded excellent agreement with experimental hydration free energy of the neutral LiF pair. Importantly for the present goals, that work followed reliable identification of local hydration structure, which led to reliable ion hydration free energies. Details of the procedure, and applications to a variety of ions, follow below.

1.2. Ions in Protein Binding Sites

Ion channels and transporters are ubiquitous, and nature has evolved a variety of membrane proteins specialized to the transport of ions such as K^+ , Na^+ , Ca^{2+} , and Mg^{2+} . The history of membrane transport proteins is now seven decades old. Yet, new ion transport proteins, structures, functions, and mechanisms of both new and old transport proteins are discovered almost daily. This makes the field of ion channels and transporters one of the most active in molecular biology (15, 35, 41, 68, 69, 70, 71, 72, 73, 74, 75, 76, 77, 78, 79, 80).

Many ion channels catalyze rapid transport (10^6 - 10^8 ions/s), while simultaneously being highly selective for a specific ion. Those two properties seem counter-intuitive. Experimental results going back to the pioneering work of Hodgkin and Keynes (81), however, indicated that ion channels that selectively catalyze rapid transport of ions have multiple sites where ions bind (15, 82). Models based on rate theory provide an intuitive explanation for the phenomenon of rapid transport facilitated by multiple binding sites (82, 83). A pre-requisite, noted earlier (14), is that ion binding relative to aqueous solution should be weak for rapid transport.

As illustrated in Figure 1, the free energy wells and barriers for rapid translocation should be minimal and centered around the free energy for ion hydration in bulk water, $\mu_{M^{q+}}^{(ex)}(\mathbf{r}) \approx \mu_{M^{q+}}^{(ex)}$. Another ion may encounter large energetic barriers ($\mu_{M^{q+}}^{(ex)}(\mathbf{r}) \gg \mu_{M^{q+}}^{(ex)}$) and, therefore, be rejected. Alternatively, the channel pore may provide a more favorable environment compared to the bulk aqueous phase ($\mu_{M^{q+}}^{(ex)}(\mathbf{r}) \ll \mu_{M^{q+}}^{(ex)}$), trapping an ion by binding tightly and hence blocking the channel.

1.2.1. Ion properties. The hydration mimicry idea originated to explain separation between ions of the same charge, but different sizes; specifically, for potassium (K) channels that conduct larger K^+ preferentially over smaller Na^+ . Ions can also be distinguished by coordination number. Comparison between the coordination structure of K^+ in a binding site and K^+ in a neighboring water-filled cavity showed both ions with 8-fold coordination (13). Earlier analysis of neutron scattering data also proposed 8 as the preferred coordination for K^+ in bulk liquid water (26, 84), though later work revised that number (26, 85, 86, 87). Altogether, these results supported the initial proposal of hydration mimicry as a mechanism for rapid and selective ion transport (12, 13, 14, 15).

1.2.2. Ligand properties. Research outside the field of membrane transport proteins has led to a variety of ideas about which ligand properties underlie preferential solvation of specific ions, but the concepts do not always account for ion binding preferences demonstrated by protein binding sites. One prominent concept attributes ligand chemistry as a key factor in ion binding preferences (88); another attributes the matching of ligand hydration free energy with ion hydration free energy (89). Recent tests of these concepts on ion binding to binding sites composed of acetate molecules found no support for the latter concept, called the “equal affinities” hypothesis. The same study reported support for the former concept, the “ligand field strength” hypothesis, but only when binding sites included the preferred number of ligands, as determined by free energy analysis. An important take-home message was that neither concept accounts for the role of the environment on binding site structure.

In proteins, the matrix surrounding binding sites, or properties of the binding sites themselves, may hinder ligand freedom to rearrange upon ion binding. Consequently, binding sites may form sub-optimal arrangements for ion binding, leading to less favorable ion binding.

Properties of a binding site that naturally take into account constraints from the environment include cavity size, or distances between ions and ligands, and the number of ligands that coordinate bound ions. While hydration mimicry is the main topic for testing here, cavity size was proposed as an initial explanation for the counter-intuitive size discrimination of K-channels, focusing attention solely on well-fitting ion-ligand distances (90, 91). In both proposals, local ion solvation structure plays the key role in ion selection and, combined with the chemistry of the ligands, compensates for ion solvation requirements for rapid permeation (70).

These factors of ligand number and cavity size echo conclusions from earlier work on ion carriers like the small molecule, valinomycin. Although valinomycin lacks a transport pathway that would require a specific binding free energy consistent with permeation (Figure 1), it does bind larger K^+ selectively over smaller Na^+ ions (92). Notably, valinomycin binds K^+ using fewer ligands than K-channels. Constraints on cavity size due to intra-molecular bonds and the surrounding solvation environment provide a compelling explanation for selective K^+ binding by valinomycin (40). In view of experimental data that characterizes K-channel binding sites as moderately inflexible when occupied by permeant ions, constrained cavity size that provides a so-called “snug fit” to permeant ions might account for selective K^+ binding by K-channels (93). A constrained cavity size, however, may inhibit transport of ions between well-fitting binding sites (28).

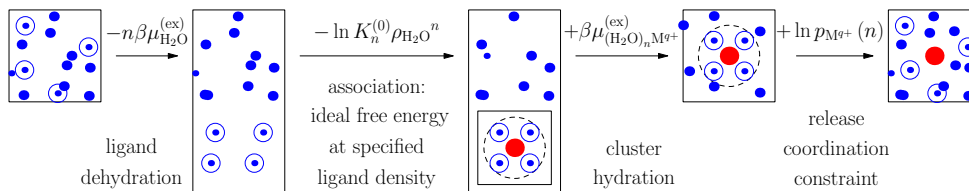


Figure 2

Hydration free energy of solute M^{q+} (red dot), interpreted on the basis of Eq. 4. The central feature of the QCT approach is analysis of the cluster $(H_2O)_n M^{q+}$.

1.3. Specific Ions and Proteins for Hydration Mimicry Analysis

Ions selected to test the hydration mimicry concept include both monovalent alkali metal ions (Li, Na, K, Rb) and divalent alkaline earth metal ions (Mg, Ca, Sr, Ba). Protein binding sites analyzed here come from a celebrated bacterial potassium-selective channel (KcsA) (15), the recently discovered bacterial magnesium-selective transporter (MgtE) (36, 94), and the voltage-gated bacterial calcium-selective channel (Ca_vAb) (37, 82).

In the results to follow, we report on the size of the local solvation structures and coordination numbers of the ions examined here. The most probable distances between ions and ligands, determined by the first maxima in radial distribution functions, and the distances reported in crystal structures, measure size. Cavity sizes should follow these quantities. The inner-shell radii, set by the first RDF maxima sets another measure of size. We discuss both of these size measures for the ions in liquid water, and compare them with ion-ligand distances in protein crystal structures for insights into hydration mimicry.

Comparisons of ion coordination properties include the number and chemistry of ligating atoms. Our main interest here for testing the hydration mimicry idea is on number of

ligating atoms that directly interact with the ion in stable complexes. Additional considerations, to be highlighted elsewhere, include the effect on ion solvation free energies from constraints on local binding site structures that may be imposed by the surrounding protein environment.

1.3.1. Specific ions. Among the monovalent ions, Na^+ and K^+ are well-known for their roles in initiating and terminating action potentials (1). As analogues to K^+ and Na^+ , Rb^+ and Li^+ are also interesting monovalent ions. In laboratory settings, Li^+ ions show contrasting rejection behaviors and Rb^+ ions permeate (38).

Among the divalent ions, Ca^{2+} and Mg^{2+} are common in biological systems. Homeostasis of these ions is tightly controlled by binding proteins, channels, exchangers, and pumps or transporters (95, 96, 97). Sr^{2+} and Ba^{2+} ions are not biologically relevant, but are well-known blockers of K^+ permeation in K-channels. These ions are used to understand the mechanism of K-channel function (17, 18, 20, 68, 98, 99). Despite close similarity in size and identical +2 charge, Ba^{2+} and Sr^{2+} exhibit different blocking behaviors in K-channels (100, 101). In particular, Ba^{2+} blocks bacterial K-channels like KcsA, but Sr^{2+} does not (19).

The comparison among ions presented here highlights patterns involving local solvation structure in water and channel binding sites among the eight ions selected for study. These ions span a range of sizes and charges. Ions of similar size include $\text{Li}^+/\text{Mg}^{2+}$ and $\text{Na}^+/\text{Ca}^{2+}$. Several ions treated here resemble K^+ in size — Rb^+ , Ba^{2+} , and Sr^{2+} .

1.3.2. Specific channels and transporters. In potassium-selective channels like the bacterial KcsA protein, crystal structures show dehydrated K^+ ions in four binding sites, S1-S4 numbered from extracellular to intracellular sides (14). Structural studies also show dehydrated Ba^{2+} in the S4 binding site of bacterial K-channels (17, 18, 20, 68). The environment varies around binding sites since water borders the ends of the selectivity filter (S1, S4) in the open state. Here, we consider an interior binding site (S2) that coordinates permeant ions with carbonyl oxygen atoms from the protein backbone. We also consider the innermost binding site located near bulk liquid water (S4), and composed of the backbone and side chain oxygens of four threonines.

Despite conservation of amino acid residues that form K-channel binding sites, the function of K-channels can change under certain conditions. The bacterial KcsA channel catalyzes rapid passage of K^+ across membranes, but rejects the smaller Na^+ ions by a high ratio of 1000:1 in physiological conditions (1). By simply changing the solution environment from high to low K^+ concentration, the 4 conserved K^+ binding sites distort so that the channel switches from a conducting configuration to a non-conducting configuration (13). In the unusual absence of K^+ , Na^+ ions can also distort the channel structure and block ion permeation (14). In related NaK channels, two sites are identical to KcsA (S3 and S4); nevertheless, both K^+ and Na^+ permeate equally well. Explanations of rapid, selective ion permeation in potassium channels should account for these intriguing observations, too.

The Ca_vAb crystal structure shows three distinct ion binding sites, with the middle one having the highest affinity. The presence of binding sites with different affinities is in good agreement with other experimental observations, and a ‘stairstep’ 3-site rate theory model can explain both the high selectivity and transport rates observed for Ca_vAb channels (82). Here, we select the middle, highest affinity Ca^{2+} binding site from Ca_vAb , which also rejects magnesium (37).

Ion comparisons: An extended sequence of simple metal ions show contrasting rejecting, permeating, and trapping behaviors.

The Mg-selective channels also contain three primary ion binding sites. While both Mg^{2+} and Ca^{2+} ions can bind to the M1 binding site, the M3 binding site selectively binds Mg^{2+} ion (94). For testing the hydration mimicry idea, we select the Mg^{2+} -selective M3 binding site from MgtE.

For the applications here, the free energy for ion binding to a channel protein, relative to its hydration free energy, is central to understanding the thermodynamic driving forces and mechanisms of ion permeation. Our tool is quasi-chemical theory (QCT), discussed in the following. QCT is a statistical mechanical theory based on close solution contacts treated at chemical resolution, by *ab initio* methods (25, 102, 103). The exploitation of chemical calculations is key to resolving ion-specificity in these problems. The coupling of structure with thermodynamics helps to understand the molecular mechanisms.

In the following, we first discuss basic aspects of QCT, including surface potentials relevant to ion hydration calculations involving interfaces, and application of QCT to protein binding sites. Then, we survey our broad set of simulation results on hydration structures for relevant metal ions in water. Next, we present our results on ion hydration free energies, obtained by analyzing local hydration structures in the QCT formulation. Finally, we compare local ion hydration structures in liquid water with local ion solvation structures in protein binding sites as a structural test of the hydration mimicry concept. We reserve for future work the comparison of ion solvation free energies in channel binding sites to ion hydration free energies. That comparison will take into account the environment surrounding the binding sites, including the possibility that the environment constrains local binding site structure (28, 104, 103).

2. QUASI-CHEMICAL THEORY

QCT was developed (25, 102, 103) for just the problems considered here: interaction free energies of specific ions in solutions and protein binding sites (29, 105, 59, 102, 103, 106, 107, 108). The excess chemical potential

$$\mu_{\text{M}^{q+}}^{(\text{ex})} = \mu_{\text{M}^{q+}} - kT \ln \rho_{\text{M}^{q+}} \Lambda_{\text{M}^{q+}}^3 \quad 1.$$

is obtained from the full chemical potential less the ideal contribution indicated. Here T is the temperature, $\rho_{\text{M}^{q+}}$ the number density of the ion of interest, and $\Lambda_{\text{M}^{q+}}$ is the thermal deBroglie wavelength (109) of species $\text{M}^{q+}(\text{aq})$. This interaction free energy analysis can also provide

$$\mu_{\text{M}^{q+}}^{(\text{ex})}(\mathbf{r}) = \mu_{\text{M}^{q+}} - kT \ln \rho_{\text{M}}(\mathbf{r}) \Lambda_{\text{M}^{q+}}^3, \quad 2.$$

describing binding at locations \mathbf{r} , generally (109).

2.1. Inner-shell Clusters

The physical concepts underlying QCT develop from consideration of association equilibria



The populations of the clusters $(\text{H}_2\text{O})_n\text{M}^{q+}$ are identified by a clustering algorithm, according to which proximal ligands of a specific M^{q+} are defined as ‘inner-shell’ partners of that ion. The theory develops by treating the cluster $(\text{H}_2\text{O})_n\text{M}^{q+}$ as a molecular component of the system.

QCT: QCT partitions the free energy into three distinct contributions based on a clustering algorithm.

QCT is then a fully elaborated statistical mechanical theory that activates modern molecular computation (25, 102, 103). What is more, QCT can be closely coordinated with molecule simulation calculations. In that way, QCT provides a compelling molecular theory of liquid water itself (110).

Thus, application of QCT begins with identification of inner-shell configurations of an ion of interest. A simple procedure is to identify those water molecules with O atoms within a distance λ from a metal ion as inner-shell partners. From there, with n water ligands in the cluster, the free energy is elaborated as

$$\mu_{M^{q+}}^{(\text{ex})} = -kT \ln K_n^{(0)} \rho_{\text{H}_2\text{O}}^n + kT \ln p_{M^{q+}}(n) + \left(\mu_{(\text{H}_2\text{O})_n M^{q+}}^{(\text{ex})} - n \mu_{\text{H}_2\text{O}}^{(\text{ex})} \right), \quad 4.$$

without statistical mechanical approximation. This formula is correct for any physical choices of λ and n . Figure 2 guides us through the several terms of Eq. 4., which we discuss in the following.

The clustering free energy for Eq. 3. is based upon the equilibrium ratio

$$K_n = \frac{p_{M^{q+}}(n)}{p_{M^{q+}}(0) \rho_{\text{H}_2\text{O}}^n}. \quad 5.$$

The factor $K_n^{(0)}$ appearing in Eq. 4. is that equilibrium constant K_n evaluated for the case that the external medium is an ideal gas. Evaluation of $K_n^{(0)}$ is accessible with widely available tools of molecular computational chemistry and can be validated against high pressure mass spectrometry data (64, 65, 111, 112, 113, 114, 115).

The ideal gas characteristic $K_n^{(0)}$ conventionally takes $p = 1$ atm, thus identifying the ideal density p/RT with $p = 1$ atm. Our applications target $\rho_{\text{H}_2\text{O}} = 1$ gm/cm³ as the density of liquid water at $T = 298$ K and $p = 1$ atm. Then $\rho_{\text{H}_2\text{O}} RT \approx 1354$ atm. These density factors describe the availability of water for binding the ion. In the application to ion hydration, this availability is enhanced by 1354 relative to the ideal $p = 1$ atm value.

Practical calculations of the outer-shell free energy term $\left(\mu_{(\text{H}_2\text{O})_n M^{q+}}^{(\text{ex})} - n \mu_{\text{H}_2\text{O}}^{(\text{ex})} \right)$ are set by adopting a statistical thermodynamic model of the environment of the $(\text{H}_2\text{O})_n M^{q+}$ cluster for the incipient free energy balance of Eq. 4. Here, we employ the polarizable continuum model (PCM) (116). With PCM, the external boundary of the cluster-solute is defined by spheres centered on each of the atoms. PCM results are sensitive to the values of the radii. But sensitivity to the values of the radii often balances-out in the free energy difference when the ion is buried by the ligands.

Finally, Figure 2 identifies the contribution $kT \ln p_M(n)$ with release of the constraint requiring n waters in ion association. The left-side of Eq. 4. is independent of n , so the complement provides $kT \ln p_M(n)$ to within a constant. Considering a specific λ , the minimum value of $kT \ln p_M(n)$ identifies the most probable n , which we denote by \bar{n} . Then we drop that statistical contribution

$$\mu_{M^{q+}}^{(\text{ex})} \approx -kT \ln K_{\bar{n}}^{(0)} \rho_{\text{H}_2\text{O}}^{\bar{n}} + \left(\mu_{(\text{H}_2\text{O})_{\bar{n}} M^{q+}}^{(\text{ex})} - \bar{n} \mu_{\text{H}_2\text{O}}^{(\text{ex})} \right). \quad 6.$$

Although \bar{n} minimizes that approximation error, the magnitude of the correction can be estimated from simulation results.

The advantage of QCT is the separation of solvation free energies into components from inner-shell and outer-shell solvent molecules, addressing the chemical physics issues in analysis of clusters. Those issues include proper overlap repulsions, polarizability, charge transfer, London dispersion interactions, n -body ligand interactions generally, distortion of flexible ligands, and zero-point motion of the cluster.

2.2. Potential of the Phase

Discussion of surface potentials brings forward the subtlety of experimental testing of computed single-ion free energies (Figure 3). To that end, we augment the free energies of Eq. 2. according to

$$\mu_{Mq+} = qe\Phi + kT \ln \rho_{Mq+} \Lambda_{Mq+}^3 + \mu_{Mq+}^{(ex)}, \quad 7.$$

by the electrostatic contribution, $qe\Phi$, for each of the conducting phases considered (117). Since Φ does not depend on chemical details of the ion, this extension plays no role in assessing the free energy of neutral combinations of ions. Φ does not depend on the ion size or structure, nor the distribution of electric charge within the ion. We will call Φ the “potential of the phase.” That quantity is determined through Poisson’s equation of electrostatics, with charge densities for the generally heterogeneous system and boundary conditions. Φ thus depends on conditions bounding and external to the phase. Considering a conducting homogeneous fluid phase, Φ is a constant throughout (118). The bulk composition is charge-neutral for such a phase.

For the case of two conducting fluid phases in equilibrium with respect to ion transfer between the phases, the difference $\Delta\Phi$ — the contact or junction potential (119) — can be tied to conditions of transfer equilibrium of ions and the neutrality of the bulk compositions (119, 120, 121, 122). For a q - q electrolyte MX,

$$2qe\Delta\Phi = -\Delta \left[\mu_{Mq+}^{(ex)} - \mu_{Xq-}^{(ex)} \right]. \quad 8.$$

The right side characteristics need not address the interface between the two phases, but are aspects of the bulk solutions for the case $\Phi = 0$ — or some other fiducial value — for each phase considered individually, as is clearly permissible.

Though the spatial transition of Φ through an interfacial region from one homogeneous conducting solution to the other is less simple, the simple result Eq. 8. was emphasized many years ago (119, 120, 121, 122) “... the junction potential in the ideal solution limits differ in general from the pure-solvent values” (119). Further, “since all real polar solvents are to some extent ionized, one has to take this effect into account in relating theory to experiments” (119). This situation does not seem to be widely appreciated.

There is broad interest in the idealized case of the fluid electrolyte solution bounded by a dielectric (non-conductor), perhaps a vacuum. This is the context for discussions of a “surface potential” (123). The solution, being a conductor, will still exhibit a spatially constant Φ . But the electrostatic potential will vary through regions bounding and exterior to the solution. The change in the electrostatic potential with passage out of the solution then requires further specification. Further theoretical modeling specifications are simpler if a sub-macroscopic cavity is imposed internally. Then the contacts of the solution with the cavity are studied (124, 125). Questions remaining include whether changes in the electrostatic potential are satisfactorily independent of cavity size and whether the electrostatic potential might be spatially constant enough to serve in the thermodynamic formulation Eq. 7. for ions with different distributions of charge.

Reserving such issues for future research (126), we finally discuss the relevance of the QCT approach, based upon Eq. 6. Since Eq. 3. is balanced with respect to charge, the K_n of Eq. 5. do not involve the potential of the phase (109). The examination of the TATB hypothesis (53, 125, 127, 128, 129, 130), and Marcus’s modeling of his tabulated values (127, 131) to depend quadratically on ion charge, make those values natural for comparison

Surface potential:
Predictions of differences between ions of the same charge are unaffected by a surface potential contribution.

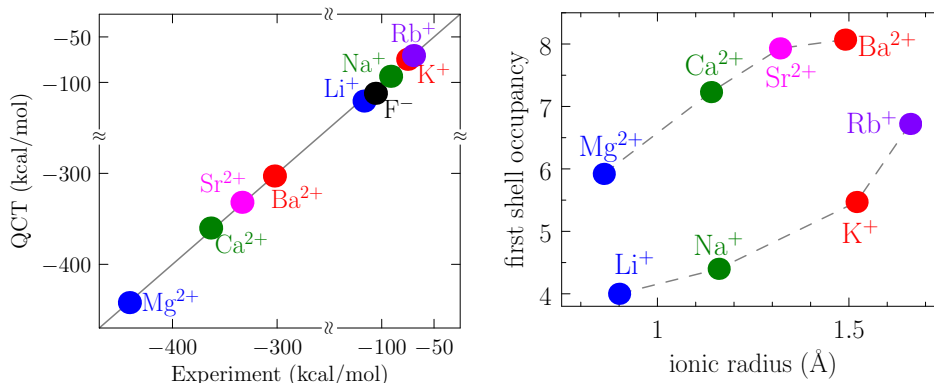


Figure 3

Left Panel: Comparison between hydration free energies calculated from QCT and the experimental tabulation of Ref.131, except for the F^- value which was updated in Ref. 133. Note that internal consistency of free energies for each collection of identically charged ions supports the view that any surface potential is treated reasonably. Right Panel: Occupancy of the nearest hydration shell defined by the minima in RDF (Figure 4) as a function of ionic radius. Water occupancy increases with increasing ion size, and water occupancy increases for divalent ions compared to monovalent ions of similar size.

with the QCT single-ion free energies that use the PCM here for the cluster free energy of Eq. 6. That the values of an alternative tabulation (132) are distinctly different is a cautionary point.

2.3. QCT and Protein Binding Sites

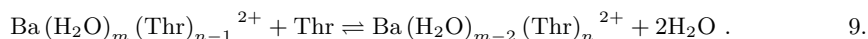
Of special interest are the ion free energies $\mu_{M^{q+}}^{(ex)}(\mathbf{r})$ at a defined binding site, as anticipated with Eq. 2. and Figure 1. QCT, being a general approach, is applicable to those problems (28, 29, 30, 62) though QCT approaches deserve further development and detailed refinement for that context.

Here we use the context of Ba^{2+} occupying the innermost binding site of K-channel (S4) to exemplify one approach. In the example, we start with the K-channel crystal structure (PDB 1K4C) and the S4 site occupied by Ba^{2+} . Four threonine (THR) amino acids interact with Ba^{2+} in bidentate fashion. Therefore, we build $Ba(Thr)_4^{2+}$ clusters, and, in fact an energy-optimized cluster structure shows all Thr O atoms displaced less than 1 Å from the crystal structure for the occupied binding site. This result is consistent with a physical intuition underlying QCT; namely (42, 102, 60), that interactions of metal ions with near-neighbors are localized, hugely stabilizing, and matters of first importance.

QCT addresses the solvation free energy of Ba^{2+} on the basis of analysis of clusters

Stability of protein binding sites to changes of water activity:

What are the probable $Ba(H_2O)_m(Thr)_{n-1}^{2+}$ coordination cases for given Thr solution concentrations?



that may form. Note that Eq. 9. makes the reasonable assumption that two H_2O molecules most naturally replace one Thr ligand. The equilibria Eq. 9., $n = 1, \dots, 4$, describe the formation of a binding site encapsulating a Ba^{2+} ion. From the beginning ($n = 1$) state to a final ($n = 4$) state, this process converts hydrated Ba^{2+} ions to Ba^{2+} ions centering a model binding site. The free energy change for this process depends on the concentrations

of the species involved, *i.e.*, a full description requires considering a standard state. We noted above with Eqs. 4. and 5. that QCT properly resolves a standard state.

The equilibria Eq. 9. can organize a solution chemistry experiment involving an aqueous solution of a Ba^{2+} electrolyte as a medium for dissolution of Thr. The dissolved concentration of Thr would be tracked, and the coordination of Ba^{2+} by the Thr would be interrogated. The question ‘what are the probable $\text{Ba}(\text{H}_2\text{O})_m(\text{Thr})_{n-1}^{2+}$ coordination cases for given Thr solution concentrations?’ would naturally arise. Alternatively expressed: from the Thr completion side of the scheme Eq. 9., how much would the H_2O activity have to increase, by dilution of the Thr, for H_2O molecules to disrupt the $(\text{Thr})_4$ binding site? Though this solution chemistry experiment would be an exceedingly natural assessment of biomolecular hydration mimicry, it has not been done as far as we know. Answers to such questions, and the natural follow-up questions, would address current issues of H_2O occupancy of potassium channels (41, 80, 134, 135).

3. ION HYDRATION STRUCTURE

Characterization of local ion hydration structure provides data essential for evaluation of the hydration mimicry concept. Radial distributions (RDFs: Figure 4) of O (water) obtained from AIMD simulations for eight metal ions in water define inner-shell structures for alkali metal ions and alkaline earth metal ions. Those AIMD results are consistent with the accurate experimental determinations of peak positions (Table 1), and with alternative studies of particular cases (136, 137, 138). These ions are often compared to investigate effects of the ion charges and sizes on channel behavior. For the smaller ions, there is an obvious separation between inner and outer hydration shells. As the ion-size increases from Li^+ to Rb^+ and Mg^{2+} to Ba^{2+} (Figure 4), the mean inner-shell occupancies become less distinct.

Neighborhood decompositions (139, 140) of those distributions characterize the natural hydration shell structure (28, 60). For the monovalent ions considered, the nearest four water molecules suffice to describe the RDF maxima even though the total occupancy of the inner shell increases with the ion size (Figure 3). Six water molecules suffice for the RDF maxima for the alkaline earth ions, but the inner-shell occupancies reach six or eight (8).

Note that sometimes a neighbor distribution can be multi-modal. See, for example, the case of $n = 6$ for $\text{K}^+(\text{aq})$ (Figure 4). We call these ‘split-shell’ cases. Since the basic development, Eq. 4., is correct independently of λ and n , we could agree to limit QCT applications to non-split-shell cases of λ and n , or we could implement the more involved computational work to treat the multi-modal occupancies directly (63).

While hydration properties of the monovalent ions have been studied extensively, fewer works have reported on the hydration properties of divalent ions. Mg^{2+} hydration has long been of biophysical interest. Dudev *et al.* (141) used electronic structure calculations to evaluate energy changes for replacing water molecules with other ligands. Six water molecules established the nominal coordination number for $\text{Mg}^{2+}(\text{aq})$ ion (108). Such results are consistent with the X-ray diffraction measurements on MgCl_2 solution (142) and our AIMD results (Figure 4).

Our RDF for Ca^{2+} ion, and its neighborhood decomposition (Figure 4), suggests that the eighth water molecule splits occupancy between inner and outer hydration shells, giving a hydration number between seven and eight (7-8). In comparison, Marcus (131) and Dudev

Split-shell coordination cases:
The 6-th nearest neighbor of $\text{K}^+(\text{aq})$ sometimes occupies an inner-most shell and, at other times, outer hydration shells.

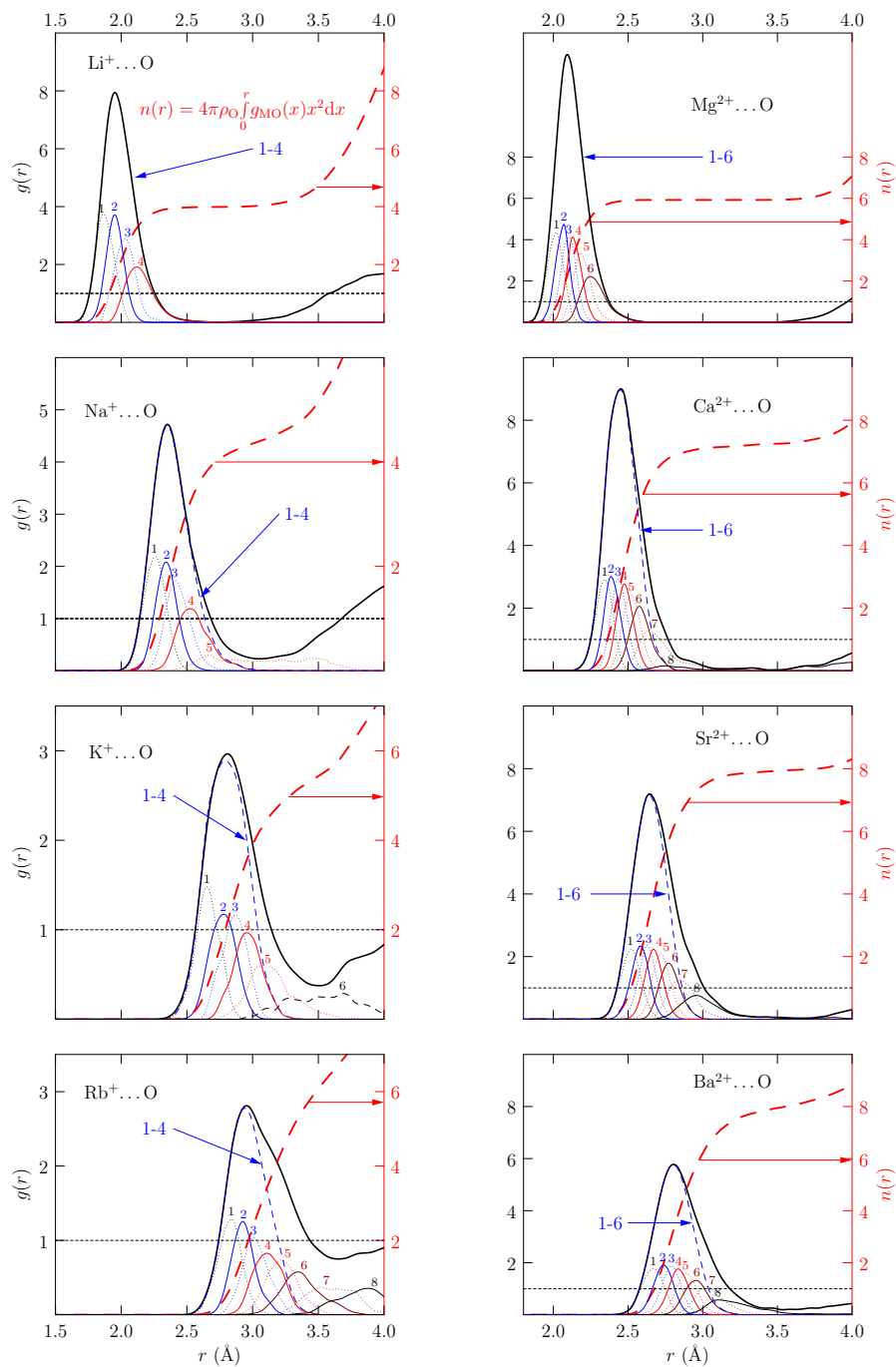


Figure 4

AIMD radial distributions of water O around eight metal ions, together with neighborhood-ordered distributions (139, 140). Red dashed curves are coordination numbers. Peak positions are given in Table 1.

Ion ⁺	AIMD	EXP	Ion ²⁺	AIMD	EXP
Li	1.95 (130, 147)	1.96 (43)	Mg	2.09 (60)	2.04 (148)
Na	2.37 (149)	2.38 (46)	Ca	2.45 (60)	2.43 (148, 150)
K	2.73 (149, 28)	2.73 (47)	Sr	2.64 (30)	2.63 (151, 152)
Rb	2.95 (42)	3.10 (153)	Ba	2.81 (59)	2.80 (154)

Table 1 Comparison of radial positions in Å of the RDF-maxima observed in AIMD simulation (Figure 4) with experimental values. References are in parentheses.

et al. (108), predicted a hydration number of 7 for Ca²⁺(aq). That possibility deserves further investigation.

Previous AIMD simulations (143, 144) calculated a mean inner-shell occupancy of 7.5 for Sr²⁺(aq), lower than values of 9.3 and 14.9 (145) from experimental work. Our result (7.9) supports the previous simulation effort. Although simulation and experiment differ in this respect, our RDF peak positions closely match the experimental results, and predictions of hydration free energy match experimental values (see below), suggesting a reliable prediction of hydration number.

An octa-coordinated hydration structure for Ba²⁺(aq) was proposed in 1933 (146). Though a several studies have interceded since, our result here lends support to that proposal and experimental data. The hydration free energy computed on that basis matches experimental results, as presented below.

4. ION HYDRATION FREE ENERGY

Ion hydration free energies set a reference value for ion permeation through protein channels and transporters. Comparisons of hydration free energies with experimental results provide baseline tests of molecular statistical thermodynamic theory. For ions, those comparisons raise the issue that hydration free energies are obtained by manipulation of neutral material combinations. Thus, tabulated single ion free energies, used here, incorporate extra-thermodynamic assumptions, and will disagree somewhat where different assumptions are used (131, 132). We respond to this issue partially here, in two different ways.

The first partial response is that computed theoretical free energies can be tested with results for neutral combinations of ions. That requires application of the theory to an example anion (44, 63, 66) in addition to the mono-atomic metal ions of primary interest here. To the extent that the theory performs satisfactorily for the neutral test case, comparisons among different cations are supported also. Figure 3 gives such an initial comparison, supported by a QCT calculation for F⁻(aq) (66, 44). Combining results for LiF produces -227.5 kcal/mol (QCT), in fair agreement with experimental tabulations, which range between -229 kcal/mol and -232 kcal/mol (132, 131, 65). This discussion is only a partial response for molecular theory because it declines advantages from dissection of a net result into physically meaningful parts, the single-ion free energies.

Our second partial response is that the theory should address the problem sufficiently thoroughly that accuracy of the individuals steps of the theory can be checked. Developing this second partial response here provides the opportunity to investigate the ingredients that are central to the performance of QCT theory.

Considering the several ingredients that are combined to evaluate the net free energy,

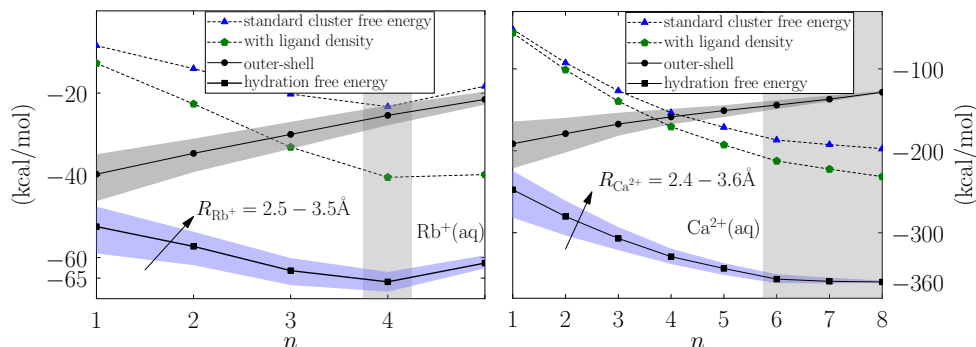


Figure 5

Dependence of individual QCT contributions on inner-shell occupancy n . Tracking $-kT \ln p(n)$, the net QCT combination is minimal for the most probable coordination number (Figure 4). For probable occupancies, the net result is insensitive to R_{Mq+} and closely agrees with the experimental tabulation of Ref. 131. The standard cluster free energy contribution at the proper ligand density (green pentagons) accounts for more than half the hydration free energy.

Ion hydration free energies: Ion hydration free energies are as large as chemical bond energies.

we base the present discussion on the examples of Rb^+ and Ca^{2+} (Figure 5). Those free energy contributions (Figure 5) are all substantial on a chemical energy scale; *i.e.*, that is, comparable to traditional chemical bond energies.

Noting the trends in each free energy contribution (Figure 5), the gas phase association term becomes more favorable with increased n for Rb^+ and Ca^{2+} . The contribution to hydration free energy from waters beyond the inner-shell clusters becomes less favorable as cluster sizes increase. That outer-shell contribution also varies with boundaries, explored here for λ set between the first maximum and minimum of the RDF for each ion. The variation with boundary becomes small upon reaching clusters with full occupancy of the inner shell, at $n=4$ for Rb^+ and $n=6-8$ for Ca^{2+} (vertical gray shading in Figure 5).

The variation of the free energy results of Figure 5 with λ and n is encouragingly simple. Nevertheless, the dielectric model for the outer-shell contributions, here PCM, can be problematic when n differs substantially from full occupancy (42). In contrast, the free energies can be satisfactory when this inner-shell occupancy is saturated because of the balance between the cluster and ligand terms of the rightmost contribution of Eq. 6.. Sensitivity to adjustment of boundaries for dielectric models is moderated then because the adjusted boundaries are somewhat buried in the cluster, though otherwise balanced. This point is significant since continuum models are typically sensitive to the boundaries, and those boundaries are not independently defined by physical principle. Indeed, boundaries (155) are "... a complicated function of density, temperature, and molecular parameters ...". Nevertheless, the rightmost (cluster) contribution of Eq. 6. is the principal theoretical approximation in QCT calculations.

Insensitivity to cavity radius of the ion: When the inner-shell is full, the cavity radius set for the ion core is less important.

5. LOCAL STRUCTURE COMPARISON

We can compare hydration structures with crystallographic data for ions in the binding sites of proteins. That structure comparison takes us another step in testing the hydration mimicry concept.

We begin with proteins permeable to Mg^{2+} and Ca^{2+} . Crystallographic data are avail-

able for recently discovered Mg-transporter structures (36, 94, 108). Compare the Mg^{2+} ion in the Mg-transporter binding site(94) (Figure 6) with a PCM-optimized structure of the $[\text{Mg}(\text{H}_2\text{O})_6]^{2+}$, composed of six waters occupying the inner solvation shell and one water in the second shell. In bulk solution (Figure 4), six inner-shell waters establish the near-neighbor distance of 2.1 Å. Unlike K-channels, where K^+ ions directly contact protein oxygen atoms, Mg^{2+} carries along its aqueous inner-shell as it occupies the protein binding site.

Similarly, the Ca_vAb structure shows a fully hydrated Ca^{2+} ion coordinated by 8 water molecules (37). These water molecules further coordinate with aspartate and asparagine side chain oxygens of the channel in the outer solvation environment. In aqueous solution, six waters establish the near-neighbor distance at 2.5 Å, though up to eight waters can be considered in broader settings (Figure 5).

Thus (Figure 6), the divalent ions observed in the crystal structures of Ca^{2+} and Mg^{2+} selective binding sites bind directly with local water molecules (156). This hydration mimicry is nearly perfect and longer-ranged effects come to the foreground with further selectivity.

In the K-selective KcsA channel, K^+ ions can occupy each of the four binding sites (S1-S4) in the selectivity filter, coordinated by eight oxygens from carbonyl groups either from the protein backbone or from threonine side chains (Figure 6) (14). The average distance between oxygen atoms and K^+ , the cavity size, is 2.8 Å. No water molecules contact K^+ in this case.

In comparison, AIMD studies of K^+ hydration structure show occupancy in the inner shell by 4-6 waters (Figure 4). The peak in the RDF saturates with four waters, located at a distance of 2.7 Å from the ion, though six waters can be considered in broader settings (Figure 5). The sixth water splits occupancy between inner and outer shells. In contrast to the eight (8) ligating oxygens in the KcsA crystal structure, in bulk solution the eighth water of hydration occupies the outer solvation volume.

The differences in K^+ contacts raise several questions. Firstly, why is the number of K^+ inner-shell O atoms less in water than in the KcsA binding site? Secondly, how can moderate transfer free energy profiles (Figure 1) arise when local structures differ? Thirdly, can local contacts account for selective binding of K^+ over Na^+ ? Prior works have addressed these questions (28, 104), and we expect they will be reviewed further in upcoming works.

Since K-selective KcsA channels select against Na^+ ions by a factor of 1000:1, the rejected ions seldom competitively occupy the KcsA pore. But in the absence of K^+ , Na^+ binds to a site in-between the K^+ binding sites (16). The Na^+ ions bind in-between sites S3 and S4, coordinated by four carbonyl oxygens arranged in a planar geometry and separated from the ion by 2.4Å.

AIMD studies indeed show Na^+ hydrated by 4-5 waters (Figure 4). The fifth water splits occupancy between inner and outer shells. Thus, when a Na^+ does enter a potassium-selective channel, the ion binds in a configuration that does mimic the bulk hydration structure. In this case, however, that binding leads to a trapped ion that blocks permeation. For the well-known K-channel blockers, Sr^{2+} and Ba^{2+} , solution hydration structures appear similar, as expected for ions of identical charge and similar size. Six waters saturate the principal maxima of the RDFs, though up to eight waters might be considered in broad settings.

Structural data for Ba^{2+} in K-channels was published recently (18), though similar data are unavailable for the Sr^{2+} ion. In that Ba^{2+} crystal structure, eight oxygen atoms from

the innermost (S4) K-channel selectivity filter constitute the binding contacts (Figure 6). With the inner-shell occupancy (8) and cavity radius (2.8Å), the protein nicely mimics the hydration environment of Ba²⁺. Structural similarity thus supports the hydration mimicry idea, but evidently the Ba²⁺ ion is too stably bound (Figure 1).

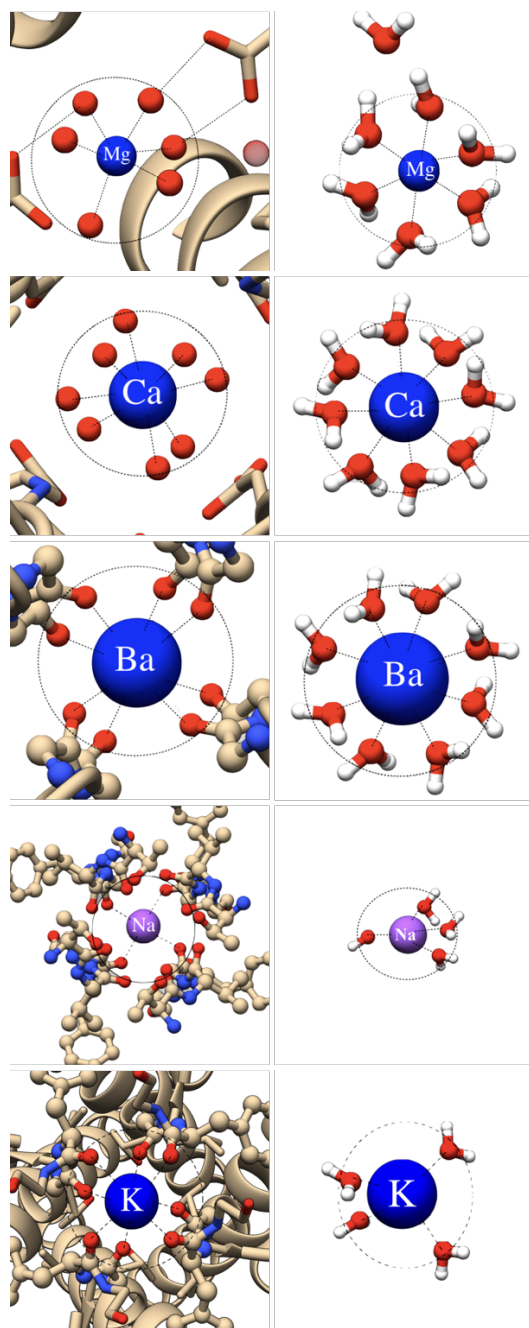


Figure 6

Comparison of solution optimized ion-water clusters (right) with X-ray crystal structures of ions inside the channels (PDB, left top to bottom, 4U9L(36), 4PDR(18), and 1K4C(13) for the bottom three). Except for the K^+ case, the ion coordination inside the channel mimics the near-neighbor hydration structure, consistent with the hydration mimicry idea.

To summarize these local structural comparisons, hydration mimicry appears applicable to all ions considered here, except for K^+ in the potassium ion channels that inspired the concept. In that case, two more O atoms contact K^+ in channel binding sites than in aqueous solution. In all other cases for which crystal structures are available, local solvation structures in crystallized channel binding sites arrange to fit each ion with contact distances and numbers anticipated from accurate solution information. In some cases, hydration mimicry leads to rapid ion permeation, but in other cases, mimicry leads to trapped ions and block of permeation.

6. CONCLUSIONS

Hydration mimicry is a long-standing idea for functional design of membrane ion channels (15). Those concepts nevertheless enter with coarse descriptors of ions and their interactions, i.e., sizes of protein binding sites and of ions, of dielectric response of the environment, and of ion binding free energies described with those coarse factors. The work described here builds the rigorous foundation for several of those factors, including ion sizes and hydration structures (Figure 3, 4). We emphasize that these primitive data, and specifically the neighborhood analyses featured in Figure 4, were not assured at the initiation of this research (24, 25, 27, 149).

Ion free energies (Figure 1) are natural assessments of those primitive descriptors and QCT (25) addresses those free energies (Figure 3), as it was designed to do (Figure 5). That theory provides a comprehensive description of the relative stability of the end-points of the ion transfer process. It also allows isolation of inner-shell (chemical contacts) and outer-shell interactions to illuminate mechanistic aspects of ion transfer. This information can be useful for designing membranes for specific phase transfer processes (7, 11).

For the membrane transport proteins assessed here, hydration mimicry applies in most, but not all, cases. Hydration mimicry applies to ions that permeate rapidly, as well as ions that block ion permeation. Nevertheless, the dynamics of the ion transfer process may also depend on the atomic-scale dynamical flexibility of the thermal systems considered (102).

SUMMARY POINTS

1. Properties that differentiate ions include size, charge, and coordination number.
2. Neighborhood analyses describe the structure of the n closest ligands to an ion, define direct contacts, and reveal 'split-shell' coordination.
3. Direct-contact structure determinations and QCT work together to seek mechanistic understanding of ion binding.
4. Interactions of metal ions with near-neighbors are as strong as chemical interactions but selectivity of ion transport depends on the balance of ion coordination equilibria, including the aqueous solution endpoints of the transport.
5. The hydration mimicry concept applies to ions that permeate rapidly and to ions that block permeation; thus, hydration mimicry does not necessarily guarantee rapid ion permeation.

FUTURE ISSUES

1. Characterize the stability of protein binding sites by manipulation of water activity. What are probable $\text{Ba}(\text{H}_2\text{O})_m(\text{Thr})_{n-1}^{2+}$ coordination cases for given Thr (threonine) solution concentrations?
2. For paradigmatic KcsA channel, are structural differences between K^+ binding in the selectivity filter and in bulk water a key to K^+/Na^+ selectivity?

7. ACKNOWLEDGMENT

We thank Thomas L. Beck for helpful discussions. Sandia National Laboratories is a multi-mission laboratory managed and operated by National Technology and Engineering Solutions of Sandia, LLC., a wholly owned subsidiary of Honeywell International, Inc., for the U.S. DOE's NNSA under contract DE-NA-0003525. This work was supported by Sandia's LDRD program and performed, in part, at the Center for Integrated NanoTechnology (CINT). This paper describes objective technical results and analysis. Any subjective views or opinions that might be expressed in the paper do not necessarily represent the views of the U.S. DOE or the U.S. Government.

LITERATURE CITED

1. Hille, B. Ionic Channels of Excitable Membranes, 3rd ed.; Sinauer Associates: Sunderland, MA, 2001.
2. Wulff, H., and Zhorov, B. S. (2008) K⁺ Channel Modulators for the Treatment of Neurological Disorders and Autoimmune Diseases. Chem. Rev. 1744–73.
3. Zhao, Y., Huang, J., Yuan, X., Peng, B., Liu, W., Han, S., and He, X. (2018) Toxins targeting the KV1.3 channel: Potential immunomodulators for autoimmune diseases. Nat. Com. 1–12.
4. Pardo, L. A., and Stuhmer, W. (2014) the Roles of K⁺ Channels in Cancer. Nat. Rev. Cancer. 39–48.
5. Banerjee, A., Lee, A., Campbell, E., and MacKinnon, R. (2013) Structure of a Pore-Blocking Toxin in Complex With a Eukaryotic Voltage-Dependent K⁺ Channel. eLife 2, ee00594.
6. Morales-Lázaro, S. L., Hernández-García, E., Serrano-Flores, B., and Rosenbaum, T. (2015) Organic Toxins as Tools to Understand Ion Channel Mechanisms and Structure. Curr. Top. Med. Chem. 15, 581–603.
7. Cygan, R., Brinker, C., Nyman, M., Leung, K., and Rempe, S. B. (2008) A Molecular Basis for Advanced Materials in Water Treatment. MRS Bull. 33, 42–47.
8. Park, H. B., Kamcev, J., Robeson, L. M., Elimelech, M., and Freeman, B. D. (2017) Maximizing the Right Stuff: The Trade-Off Between Membrane Permeability and Selectivity. Science 356, eaab0530.
9. Tang, C. Y., Zhao, Y., Wang, R., Hélix-Nielsen, C., and Fane, A. G. (2012) Desalination by Biomimetic Aquaporin Membranes: Review of Status and Prospects. Desal. 308, 34–40.
10. Hélix-Nielsen, C. (2018) Biomimetic Membranes as a Technology Platform: Challenges and Opportunities. Membranes (Basel) 8, 44.
11. Fu, Y., Jiang, Y.-B., Dunphy, D., Xiong, H., Coker, E., Chou, S., Zhang, H., Vanegas, J. M., Croissant, J. G., Cecchi, J. L., Rempe, S. B., and Brinker, C. J. (2018) Ultra-Thin Enzymatic Liquid Membrane for CO₂ Separation and Capture. Nat. Commun. 1–12.
12. Doyle, D., Morais Cabral, J., Pfuetzner, R. A., Kuo, A., Gulbis, J. M., Cohen, S. L., Chait, B. T., and MacKinnon, R. (1998) The Structure of the Potassium Channel: Molecular Basis of K⁺ Conduction and Selectivity. Science (New York, N.Y.) 280, 69.
13. Zhou, Y., Morais-Cabral, J., Kaufman, A., and MacKinnon, R. (2001) Chemistry of Ion Coordination and Hydration Revealed by a K⁺ Channel-Fab Complex at 2.0Å Resolution. Nature 414, 43–48.
14. MacKinnon, R. (2003) Minireview: Potassium channels. FEBS letters 555, 62–65.
15. MacKinnon, R. (2004) Potassium Channels and the Atomic Basis of Selective Ion Conduction (Nobel Lecture). Angew. Chemie Int. Ed. 43, 4265–4277.
16. Asthagiri, D., Pratt, L. R., and Paulaitis, M. E. (2006) Role of Fluctuations in a Snug-Fit Mechanism of KcsA Channel Selectivity. J. Chem. Phys. 125, 24701.
17. Jiang, Y., and MacKinnon, R. (2000) The Barium Site in a Potassium Channel by X-Ray Crystallography. J. Gen. Phys. 115, 269.
18. Lam, Y. L., Zeng, W., Sauer, D., and Jiang, Y. (2014) The Conserved Potassium Channel Filter can have Distinct Ion Binding Profiles: Structural Analysis of Rubidium, Cesium, and Barium Binding in NaK2K. J. Gen. Phys. 144, 181–192.
19. Piasta, K. N., Theobald, D. L., and Miller, C. (2011) Potassium-Selective Block of Barium Permeation Through Single KcsA Channels. J. Gen. Phys. 138, 421–436.
20. Guo, R., Zeng, W., Cui, H., Chen, L., and Ye, S. (2014) Ionic Interactions of Ba²⁺ Blockades in the MthK K⁺ Channel. J. Gen. Phys. 144, 193–200.
21. Rempe, S. B. et al. (2010) Computational and Experimental Platform for Understanding and Optimizing Water Flux and Salt Rejection in Nanoporous Membranes. SANDIA Report, SAND2010-6735
22. Rempe, S., Brinker, C. J., Rogers, D. M., Jiang, Y.-B., and Yang, S. Biomimetic Membranes and Methods of Making Biomimetic Membranes. 2016; US Patent 9,486,742.

23. Pohorille, A., and Pratt, L. R. (2012) Is Water the Universal Solvent for Life? *Origins of Life and Evolution of Biospheres* **42**, 405–409.
24. Rempe, S. B., Pratt, L. R., Hummer, G., Kress, J. D., Martin, R. L., and Redondo, A. (2000) The Hydration Number of Li^+ in Liquid Water. *J. Am. Chem. Soc.* **122**, 966–967.
25. Pratt, L. R., and Rempe, S. B. *Simulation and Theory of Electrostatic Interactions in Solution*; AIP Publishing, 1999; Vol. 492; pp 172–201.
26. Varma, S., and Rempe, S. B. (2006) Coordination Numbers of Alkali Metal Ions in Aqueous Solutions. *Biophys. Chem.* **124**, 192–199.
27. Mason, P. E., Ansell, S., Neilson, G., and Rempe, S. B. (2015) Neutron Scattering Studies of the Hydration Structure of Li^+ . *J. Phys. Chem. B* **119**, 2003–2009.
28. Varma, S., and Rempe, S. B. (2007) Tuning Ion Coordination Architectures to Enable Selective Partitioning. *Biophys. J.* **93**, 1093–1099.
29. Stevens, M. J., and Rempe, S. L. B. (2016) Ion-Specific Effects in Carboxylate Binding Sites. *J. Phys. Chem. B* **120**, acs.jpcc.6b10641.
30. Chaudhari, M. I., and Rempe, S. B. (2018) Strontium and Barium in Aqueous Solution and a Potassium Channel Binding Site. *J. Chem. Phys.* **148**, 222831.
31. Miller, C. (1982) Coupling of Water and Ion Fluxes in a K^+ -Selective Channel of Sarcoplasmic Reticulum. *Biophys. J.* **38**, 227–230.
32. Alcayaga, C., Cecchi, X., Alvarez, O., and Latorre, R. (1989) Streaming Potential Measurements in Ca^{2+} -Activated K^+ Channels From Skeletal and Smooth Muscle. Coupling of Ion and Water Fluxes. *Biophys. J.* **55**, 367–371.
33. Iwamoto, M., and Oiki, S. (2011) Counting Ion and Water Molecules in a Streaming File through the Open-Filter Structure of the K Channel. *J. Neurosci.* **31**, 12180–12188.
34. Armstrong, C. (2015) Packaging Life: The Origin of Ion-Selective Channels. *Biophys. J.* **109**, 173–177.
35. Roux, B. (2005) Ion Conduction and Selectivity in K^+ Channels. *Annu. Rev. Biophys. Biomol. Struct.* **34**, 153–171.
36. Payandeh, J., Pfoh, R., and Pai, E. F. (2013) The Structure and Regulation of Magnesium Selective Ion Channels. *BBA - Biomembranes* **1828**, 2778–2792.
37. Tang, L., Gamal El-Din, T. M., Payandeh, J., Martinez, G. Q., Heard, T. M., Scheuer, T., Zheng, N., and Catterall, W. A. (2014) Structural Basis for Ca^{2+} Selectivity of a Voltage-gated Calcium Channel. *Nature* **505**, 56–61.
38. Lockless, S. W., Zhou, M., and MacKinnon, R. (2007) Structural and Thermodynamic Properties of Selective Ion Binding in a K^+ Channel. *PLoS biology* **5**, e121.
39. Valiyaveetil, F., Leonetti, M., Muir, T. W., and MacKinnon, R. (2006) Ion Selectivity in a Semisynthetic K^+ Channel Locked in the Conductive Conformation. *Science (New York, N.Y.)* **314**, 1004–1007.
40. Varma, S., Sabo, D., and Rempe, S. B. (2008) K^+/Na^+ Selectivity in K Channels and Valinomycin: Over-coordination Versus Cavity-size constraints. *J. Mol. Bio.* **376**, 13–22.
41. Tilegenova, C., Cortes, D. M., Jahovic, N., Hardy, E., Hariharan, P., Guan, L., and Cuello, L. G. (2019) Structure, Function, and Ion-Binding Properties of a K^+ Channel Stabilized in the 2, 4-Ion-Bound Configuration. *Proc. Nat. Acad. Sci. USA* **201901888**.
42. Sabo, D., Jiao, D., Varma, S., Pratt, L. R., and Rempe, S. B. (2013) Case Study of $\text{Rb}^+(\text{aq})$, Quasi-Chemical Theory of Ion Hydration, and the No Split Occupancies Rule. *Ann. Rep. Prog. Chem., Sect. C (Phys. Chem.)* **109**, 266–278.
43. Mason, P. E., Ansell, S., Neilson, G., and Rempe, S. B. (2015) Neutron Scattering Studies of the Hydration Structure of Li^+ . *J. Phys. Chem. B* **119**, 2003–2009.
44. Muralidharan, A., Pratt, L. R., Chaudhari, M. I., and Rempe, S. B. (2018) Quasi-Chemical Theory With Cluster Sampling From *Ab Initio* Molecular Dynamics: Fluoride ($\text{F}^-(\text{aq})$) Anion Hydration. *J. Phys. Chem. A* **122**, 9806–9812.
45. Fulton, J. L., Heald, S. M., Badyal, Y. S., and Simonson, J. M. (2003) Understanding the

- Effects of Concentration on the Solvation Structure of Ca^{2+} in Aqueous Solution. I: The Perspective on Local Structure from EXAFS and XANES. *J. Phys. Chem. A* **107**, 4688–4696.
46. Galib, M., Baer, M. D., Skinner, L. B., Mundy, C. J., Huthwelker, T., Schenter, G. K., Benmore, C. J., Govind, N., and Fulton, J. L. (2017) Revisiting the Hydration Structure of Aqueous Na^+ . *J. Chem. Phys.* **146**, 84504.
 47. Glezakou, V. A., Chen, Y., Fulton, J. L., Schenter, G. K., and Dang, L. X. (2006) Electronic Structure, Statistical Mechanical Simulations, and EXAFS Spectroscopy of Aqueous Potassium. *Theor. Chem. Acc.* **115**, 86–99.
 48. Kirchner, B., di Dio, P. J., and Hutter, J. *Multiscale Molecular Methods in Applied Chemistry*; Springer, 2011; pp 109–153.
 49. Lyubartsev, A. P., Laasonen, K., and Laaksonen, A. (2001) Hydration of Li^+ Ion. An Ab Initio Molecular Dynamics Simulation. *J. Chem. Phys.* **114**, 3120–3126.
 50. Heuft, J. M., and Meijer, E. J. (2005) Density Functional Theory Based Molecular-Dynamics Study of Aqueous Fluoride Solvation. *J. Chem. Phys.* **122**, 94501.
 51. Whitfield, T. W., Varma, S., Harder, E., Lamoureux, G., Rempe, S. B., and Roux, B. (2007) Theoretical Study of Aqueous Solvation of K^+ Comparing *ab initio*, polarizable, and fixed-charge models. *J. Chem. Theo. Comp.* **3**, 2068–2082.
 52. Bankura, A., Santra, B., Jr., R. A. D., Swartz, C. W., Klein, M. L., and Wu, X. (2015) A Systematic Study of Chloride Ion Solvation in Water Using Van Der Waals Inclusive Hybrid Density Functional Theory. *Mol. Phys.* **113**, 2842–2854.
 53. Leśniewski, M., and Śmiechowski, M. (2018) Communication: Inside the Water Wheel: Intrinsic Differences Between Hydrated Tetraphenylphosphonium and Tetraphenylborate Ions. *J. Chem. Phys.* **149**, 171101–6.
 54. Sharma, B., and Chandra, A. (2018) Nature of Hydration Shells of a Polyoxy-Anion With a Large Cationic Centre: The Case of Iodate Ion in Water. *J. Comput. Chem.* **39**, 1226–1235.
 55. Zhou, L., Xu, J., Xu, L., and Wu, X. (2019) Importance of Van Der Waals Effects on the Hydration of Metal Ions From the Hofmeister Series. *J. Chem. Phys.* **150**, 124505.
 56. Karmakar, A. (2019) Ab Initio Molecular Dynamics Simulation of Supercritical Aqueous Ionic Solutions: Spectral Diffusion of Water in the Vicinity of Br^- and I^- Ions. *J. Mol. Liq.* **279**, 306–316.
 57. Martinek, T., Duboué-Dijon, E., Timr, Š., Mason, P. E., Baxová, K., Fischer, H. E., Schmidt, B., Pluhařová, E., and Jungwirth, P. (2018) Calcium Ions in Aqueous Solutions: Accurate Force Field Description Aided by Ab Initio Molecular Dynamics and Neutron Scattering. *J. Chem. Phys.* **148**, 222813.
 58. Rempe, S. B., Asthagiri, D., and Pratt, L. R. (2004) Inner shell definition and absolute hydration free energy of $\text{K}^+(\text{aq})$ on the Basis of Quasi-Chemical Theory and *ab initio* Molecular Dynamics. *Phys. Chem. Chem. Phys.* **6**, 1966.
 59. Chaudhari, M. I., Soniat, M., and Rempe, S. B. (2015) Octa-Coordination and the Aqueous Ba^{2+} Ion. *J. Phys. Chem. B* **119**, 8746–8753.
 60. Chaudhari, M. I., Pratt, L. R., and Rempe, S. B. (2017) Utility of chemical computations in predicting solution free energies of metal ions. *Mol. Sim.* 1–7.
 61. Varma, S., and Rempe, S. B. (2010) Multibody Effects in ion Binding and Selectivity. *Biophys. J.* **99**, 3394–3401.
 62. Rossi, M., Tkatchenko, A., Rempe, S. B., and Varma, S. (2013) Role of Methyl-Induced Polarization in Ion Binding. *Proc. Nat. Ac. Sci.* **110**, 12978–12983.
 63. Muralidharan, A., Pratt, L. R., Chaudhari, M. I., and Rempe, S. B. (2019) Quasi-Chemical Theory for Anion Hydration and Specific Ion Effects: $\text{Cl}^-(\text{Aq})$ vs. $\text{F}^-(\text{Aq})$. *Chem. Phys. Letts.: X* **4**, 100037.
 64. Peschke, M., Blades, A. T., and Kebarle, P. (1998) Hydration Energies and Entropies for Mg^{2+} , Ca^{2+} , Sr^{2+} , and Ba^{2+} from Gas-Phase Ion-Water Molecule Equilibria Determinations. *J. Phys. Chem. A* **102**, 9978–9985.

65. Tissandier, M. D., Cowen, K. A., Feng, W. Y., Gundlach, E., Cohen, M. H., Earhart, A. D., Coe, J. V., and Tuttle, T. R. (1998) the Proton's Absolute Aqueous Enthalpy and Gibbs Free Energy of Solvation From Cluster-Ion Solvation Data. *J. Phys. Chem. A* **102**, 7787–7794.
66. Chaudhari, M. I., Rempe, S. B., and Pratt, L. R. (2017) Quasi-chemical Theory of $F^{-}(aq)$: The No Split Occupancies Rule Revisited. *J. Chem. Phys.* **147**, 161728.
67. Robertson, W. H., and Johnson, M. A. (2003) Molecular Aspects of Halide Ion Hydration: The Cluster Approach. *Annu Rev Phys Chem* **54**, 173–213.
68. Lockless, S., Zhou, M., and MacKinnon, R. (2007) Structural and Thermodynamic Properties of Selective Ion Binding in a K^{+} Channel. *PLoS Bio.* **5**, e121.
69. Morais-Cabral, J. H., Zhou, Y., and MacKinnon, R. (2001) Energetic Optimization of Ion Conduction Rate by the K^{+} Selectivity Filter. *Nature* **414**, 37–42.
70. Gouaux, E., and MacKinnon, R. (2005) Principles of Selective Ion Transport in Channels and Pumps. *Science* **310**, 1461.
71. Beckstein, O., Biggin, P. C., Bond, P., Bright, J. N., Domene, C., Grottesi, A., Holyoake, J., and Sansom, M. S. P. (2003) Ion Channel Gating: Insights via Molecular Simulations. *FEBS Letts.* **555**, 85–90.
72. Catterall, W. A. (2011) Voltage-Gated Calcium Channels. *Cold Spring Harbor Perspectives in Biology* **3**, a003947–a003947.
73. Payandeh, J., Pfoh, R., and Pai, E. F. (2013) The Structure and Regulation of Magnesium Selective Ion Channels. *BBA - Biomembranes* **1828**, 2778–2792.
74. Kratochvil, H. T., Carr, J. K., Matulef, K., Li, H., Maj, M., Ostmeier, J., Serrano, A. L., Raghuraman, H., Moran, S. D., Skinner, J. L., Perozo, E., Roux, B., Valiyaveetil, F. I., and Zanni, M. T. (2016) Instantaneous Ion Configurations in the K^{+} Configurations in the K^{+} Ion Channel Selectivity Filter Revealed by 2D IR Spectroscopy. *Science* **353**, 1040–1044.
75. Cuello, L. G., Cortes, D. M., and Perozo, E. (2017) The gating cycle of a K^{+} channel at atomic resolution. *eLife* **6**, e28032.
76. Last, N. B., Sun, S., Pham, M. C., and Miller, C. (2017) Molecular Determinants of Permeation in a Fluoride-Specific Ion Channel. *eLife* **6**, e31259.
77. Shlosman, I., Marinelli, F., Faraldo-Gómez, J. D., and Mindell, J. A. (2018) the Prokaryotic Na^{+}/Ca^{2+} Exchanger NCX_Mj Transports Na^{+} and Ca^{2+} in a 3: 1 Stoichiometry. *J. Gen. Phys.* **150**, 51–65.
78. Kshatri, A. S., Gonzalez-Hernandez, A. J., and Giraldez, T. (2018) Functional Validation of Ca^{2+} -Binding Residues From the Crystal Structure of the BK Ion Channel. *Biochimica et Biophysica Acta (BBA) - Biomembranes* **1860**, 943–952.
79. Tong, A., Petroff, J. T., Hsu, F.-F., Schmidpeter, P. A. M., Nimigeon, C. M., Sharp, L., Brannigan, G., and Cheng, W. W. L. (2019) Direct Binding of Phosphatidylglycerol at Specific Sites Modulates Desensitization of a Pentameric Ligand-Gated Ion Channel. *bioRxiv*
80. Oster, C., Hendricks, K., Kopec, W., Chevelkov, V., Shi, C., Michl, D., Lange, S., Sun, H., deGroot, B. L., and Lange, A. (2019) the Conduction Pathway of Potassium Channels Is Water Free Under Physiological Conditions. *Science Advances* **5**, 1–8.
81. Hodgkin, A. L., and Keynes, R. D. (1955) The Potassium Permeability of a Giant Nerve Fibre. *J. Physiol. (Lond.)* **128**, 61–88.
82. Sather, W. A., and McCleskey, E. W. (2003) Permeation and Selectivity in Calcium Channels. *Ann. Rev. Physiol.* **65**, 133–159.
83. Dang, T. X., and McCleskey, E. W. (1998) Ion Channel Selectivity through Stepwise Changes in Binding Affinity. *J. Gen. Physiol.* **111**, 185–193.
84. Ohtomo, N., and Arakawa, K. (1980) Neutron Diffraction Study of Aqueous Ionic Solutions. II. Aqueous Solutions of Sodium Chloride and Potassium Chloride. *Bull Chem Soc Jpn* **53**, 1789.
85. Mason, P. E., Sullivan, D., Neilson, G., and Ramos, S. (2001) Neutron and X-ray Scattering Studies of Hydration in Aqueous Solutions. *Phil. Trans. R. Soc. Lond Ser. A: Math. Phys.*

- Eng. Sci. **359**, 1575–1591.
86. Soper, A. K., and Weckström, K. (2006) Ion Solvation and Water Structure in Potassium Halide Aqueous Solutions. Biophysical chemistry **124**, 180–191.
 87. Mancinelli, R., Botti, A., Bruni, F., Ricci, M. A., and Soper, A. K. (2007) Hydration of Sodium, Potassium, and Chloride Ions in Solution and the Concept of Structure Maker/Breaker. J. Phys. Chem. B **111**, 13570–13577.
 88. Eisenman, G., and Horn, R. (1983) the Role of Kinetic and Equilibrium Processes in Ion Permeation Through Channels. J. Membr. Biol. **76**, 197–225.
 89. Collins, K. D. (1997) Density-Dependent Strength of Hydration and Biological Structure. Biophys J **72**, 65–76.
 90. Armstrong, C. M., and Taylor, S. R. (1980) Interaction of Barium Ions with Potassium Channels in Squid Giant Axons. Biophys. J. **473**–488.
 91. Armstrong, C. M., Swenson, R. P., and Taylor, S. R. (1982) Block of Squid Axon K-channels by Internally and Externally Applied Barium Ions. J. Gen. Phys. **80**, 663–682.
 92. Neupert-Laves, K., and Dobler, M. (1975) The Crystal Structure of a K^+ Complex of Valinomycin. Helvetica Chimica Acta **58**, 432–442.
 93. Bhate, M. P., Wylie, B. J., Tian, L., and McDermott, A. E. (2010) Conformational Dynamics in the Selectivity Filter of KcsA in Response to Potassium Ion Concentration. J. Molec. Bio. **401**, 155–166.
 94. Takeda, H., Hattori, M., Nishizawa, T., Yamashita, K., Shah, S. T. A., Caffrey, M., Maturana, A. D., Ishitani, R., and Nureki, O. (2014) Structural basis for ion selectivity revealed by high-resolution crystal structure of Mg(2+) channel MgtE. Nat Commun **5**, 5374.
 95. Verkhatsky, A., and Parpura, V. (2014) Calcium Signalling and Calcium Channels Evolution and General Principles. Eu. J. Pharm. **739**, 1–3.
 96. Carafoli, E. (1987) Intracellular Calcium Homeostasis. Annu. Rev. Biochem. **56**, 395–433.
 97. Romani, A. M. P. (2011) Cellular Magnesium Homeostasis. Arch. Biochem. Biophys. **512**, 1–23.
 98. Armstrong, C. M., and Palti, Y. (1991) Potassium Channel Block by Internal Calcium and Strontium. J. Gen. Phys. **97**, 627–638.
 99. Elinder, F., Madeja, M., and Arhem, P. (1996) Surface Charges of K channels. Effects of Strontium on Five Cloned Channels Expressed in Xenopus Oocytes. J. Gen. Phys. **108**, 325–332.
 100. Sugihara, I. (1998) Activation and Two Modes of Blockade by Strontium of Ca^{2+} -Activated K^+ Channels in Goldfish Saccular-Hair Cells. J. Gen. Physiol. **111**, 363–379.
 101. Soh, H., and Park, C. S. (2002) Localization of Divalent Cation-Binding Site in the Pore of a Small Conductance Ca^{2+} -Activated K^+ Channel and Its Role in Determining Current-Voltage. Biophys. J. **83**, 2528–2538.
 102. Asthagiri, D., Dixit, P., Merchant, S., Paulaitis, M., Pratt, L., Rempe, S. B., and Varma, S. (2010) Ion Selectivity From Local Configurations of Ligands in Solutions and Ion Channels. Chem. Phys. Letts. **485**, 1–7.
 103. Rogers, D. M., and Rempe, S. B. (2011) Probing the Thermodynamics of Competitive Ion Binding Using Minimum Energy Structures. J. Phys. Chem. B **115**, 9116–9129.
 104. Varma, S., Rogers, D. M., Pratt, L. R., and Rempe, S. B. (2011) Design Principles for K^+ Selectivity in Membrane Transport. J. Gen. Phys. **137**, 479–488.
 105. Asthagiri, D., Pratt, L. R., Paulaitis, M. E., and Rempe, S. B. (2004) Hydration Structure and Free Energy of Biomolecularly Specific Aqueous Dications, Including Zn^{2+} and First Transition Row Metals. J. Am. Chem. Soc. **126**, 1285–1289.
 106. Asthagiri, D., Pratt, L. R., and Ashbaugh, H. S. (2003) Absolute Hydration Free Energies of Ions, Ion–water Clusters, and Quasichemical Theory. J. Chem. Phys. **119**, 2702–2708.
 107. Jiao, D., and Rempe, S. B. (2012) Combined Density Functional Theory (DFT) and Continuum Calculations of p Kain Carbonic Anhydrase. Biochemistry **51**, 5979–5989.

108. Dudev, T., and Lim, C. (2013) Importance of Metal Hydration on the Selectivity of Mg^{2+} versus Ca^{2+} in Magnesium Ion Channels. *J. Am. Chem. Soc.* **135**, 17200–17208.
109. Beck, T. L., Paulaitis, M. E., and Pratt, L. R. The Potential Distribution Theorem and Models of Molecular Solutions; Cambridge University Press, 2006.
110. Shah, J., Asthagiri, D., Pratt, L., and Paulaitis, M. (2007) Balancing Local Order and Long-ranged Interactions in the Molecular Theory of Liquid Water. *J. Chem. Phys.* **127**, 144508.
111. Kebarle, P. (1977) Ion Thermochemistry and Solvation from Gas Phase Ion Equilibria. *Ann. Rev. Phys. Chem.* **28**, 445–476.
112. Keesee, R. G., and Castleman Jr, A. W. (1980) Gas-Phase Studies of Hydration Complexes of Cl^- and I^- and Comparison to Electrostatic Calculations in the Gas Phase. *Chem. Phys. Letts.* **74**, 139–142.
113. Keesee, R. G., Lee, N., and Castleman Jr, A. W. (1980) Properties of Clusters in the Gas Phase: V. Complexes of Neutral Molecules onto Negative Ions. *J. Chem. Phys.* **73**, 2195–2202.
114. Castleman, A. W., and Keesee, R. G. (1986) Ionic Clusters. *Chem. Rev.* **86**, 589–618.
115. Castleman Jr, A. W., and Keesee, R. G. (1988) Gas-Phase Clusters: Spanning the States of Matter. *Science* **241**, 36–42.
116. Tomasi, J., Mennucci, B., and Cammi, R. (2005) Quantum Mechanical Continuum Solvation Models. *Chem. Rev.* **105**, 2999–3093.
117. Pethica, B. A. (2007) Are Electrostatic Potentials Between Regions of Different Chemical Composition Measurable? The Gibbs–Guggenheim Principle Reconsidered, Extended and Its Consequences Revisited. *Phys. Chem. Chem. Phys.* **9**, 6253–6262.
118. Landau, L. D., and Lifshitz, E. M. Electrodynamics of Continuous Media; Course in Theoretical Physics; Pergamon Press, 1960; Vol. 8, §1.
119. Zhou, Y., Stell, G., and Friedman, H. L. (1988) Note on Standard Free Energy of Transfer and Partitioning of Ionic Species Between Two Fluid Phases. *J. Chem. Phys.* **89**, 3836–3839.
120. Nichols, A. L., and Pratt, L. R. (1984) Salt effects on the Surface Tensions of Dilute Electrolyte Solutions: The Influence of Nonzero Relative Solubility of the Salt Between the Coexisting Phases. *J. Chem. Phys.* **80**, 6225–6233.
121. Pratt, L. R. (1992) Contact Potentials of Solution Interfaces: Phase Equilibrium and Interfacial Electric Fields. *J. Phys. Chem* **96**, 25–33.
122. You, X., Chaudhari, M. I., and Pratt, L. R. Aqua Incognita: Why Ice Floats on Water and Galileo 400 Years on; Connor Court Press Ballarat, 2014; pp 434–442, Comparison of Mechanical and Thermodynamical Evaluations of Electrostatic Potential Differences between Electrolyte Solutions.
123. Lyklema, J. (2017) View of Interfacial Potentials: Measuring the Immeasurable? *Substantia* **1**, 75–93.
124. Beck, T. L. (2013) The Influence of Water Interfacial Potentials on Ion Hydration in Bulk Water and Near Interfaces. *Chem. Phys. Letts.*
125. Pollard, T. P., and Beck, T. L. (2018) Re-examining the Tetraphenyl-arsonium/Tetraphenylborate (TATB) Hypothesis for Single-ion Solvation Free Energies. *J. Chem. Phys.* **148**, 222830.
126. Doyle, C., Shi, Y., and Beck, T. L. (2019) The Importance of the Water Molecular Quadrupole for Estimating Interfacial Potential Shifts Acting on Ions Near the Liquid-Vapor Interface. [preprint](#)
127. Marcus, Y. (1987) The Thermodynamics of Solvation of Ions. Part 4.—Application of the Tetraphenylarsonium Tetraphenylborate (TATB) Extrathermodynamic Assumption to the Hydration of Ions and to Properties of Hydrated Ions. *J. Chem. Soc., Faraday Trans. 1: Phys. Chem. Cond. Phases* **83**, 2985–2992.
128. Schurhammer, R., and Wipff, G. (2000) Are the Hydrophobic AsPh_4^+ and BPh_4^- Ions Equally Solvated? A Theoretical Investigation in Aqueous and Nonaqueous Solutions Using Different Charge Distributions. *J. Phys. Chem. A* **104**, 11159–11168.
129. Duignan, T. T., Baer, M. D., and Mundy, C. J. (2018) Understanding the Scale of the Single

- Ion Free Energy: A Critical Test of the Tetra-phenyl Arsonium and Tetra-phenyl Borate Assumption. *J. Chem. Phys.* **148**, 222819.
130. Leung, K., Rempe, S. B., and von Lilienfeld, O. A. (2009) *Ab initio* Molecular Dynamics Calculations of Ion Hydration Free Energies. *J. Chem. Phys.* **130**, 204507.
 131. Marcus, Y. (1994) A Simple Empirical Model Describing the Thermodynamics of Hydration of Ions of Widely Varying Charges, Sizes, and Shapes. *Biophys. Chem.* **51**, 111–127.
 132. Friedman, H., and Krishnan, C. *Aqueous Solutions of Simple Electrolytes*; Springer, 1973; pp 1–118.
 133. Marcus, Y. *Ions in Solution and their Solvation*; John Wiley & Sons, 2015.
 134. Hummer, G. (2014) Potassium Ions Line Up. *Science* **346**, 303–303.
 135. Kopec, W., and de Groot, B. L. (2019) Molecular Simulations of Ion Permeation, Gating and Selectivity in K^+ Channels. *Biophys. J.* **116**, 16a.
 136. Jiao, D., King, C., Grossfield, A., Darden, T. A., and Ren, P. (2006) Simulation of Ca^{2+} and Mg^{2+} Solvation Using Polarizable Atomic Multipole Potential. *J. Phys. Chem. B* **110**, 18553–18559.
 137. Mehandzhyski, A. Y., Riccardi, E., van Erp, T. S., Trinh, T. T., and Grimes, B. A. (2015) *Ab Initio* Molecular Dynamics Study on the Interactions between Carboxylate Ions and Metal Ions in Water. *J. Phys. Chem. B* **119**, 10710–10719.
 138. Soniat, M., Hartman, L., and Rick, S. W. (2015) Charge Transfer Models of Zinc and Magnesium in Water. *J. Chem. Theory Comput.* **11**, 1658–1667.
 139. Mazur, S. (1992) Neighborhood Partition of the Radial Distribution Function for Simple Liquids. *J. Chem. Phys.* **97**, 9276.
 140. Zhu, P., You, X., Pratt, L., and Papadopoulos, K. (2011) Generalizations of the Fuoss Approximation for Ion Pairing. *J. Chem. Phys.* **134**, 54502.
 141. Dudev, T., Cowan, J. A., and Lim, C. (1999) Competitive Binding in Magnesium Coordination Chemistry: Water versus Ligands of Biological Interest. *J. Am. Chem. Soc.* **121**, 7665–7673.
 142. Caminiti, R., Licheri, G., Piccaluga, G., and Pinna, G. (1979) X-ray Diffraction Study of $MgCl_2$ Aqueous Solutions. *J. Appl. Cryst.* **12**, 34–38.
 143. Harris, D. J., Brodholt, J. P., and Sherman, D. M. (2003) Hydration of Sr^{2+} in Hydrothermal Solutions from *ab initio* Molecular Dynamics. *J. Phys. Chem. B* **107**, 9056–9058.
 144. Spohr, E., Palinkas, G., Heinzinger, K., Bopp, P., and Probst, M. M. (2002) Molecular Dynamics Study of an Aqueous Strontium Chloride Solution. *J. Phys. Chem.* **92**, 6754–6761.
 145. Ohtaki, H., and Radnai, T. (1993) Structure and Dynamics of Hydrated Ions. *Chem. Rev.* **93**, 1157–1204.
 146. Bernal, J. D., and Fowler, R. H. (1933) A Theory of Water and Ionic Solution, with Particular Reference to Hydrogen and Hydroxyl Ions. *J. Chem. Phys.* **1**, 515–548.
 147. Alam, T. M., Hart, D., and Rempe, S. L. B. (2011) Computing the 7Li NMR Chemical Shielding of Hydrated Li^+ Using Cluster Calculations and Time-Averaged Configurations from *ab-initio* Molecular Dynamics Simulations. *Phys. Chem. Chem. Phys.* **13**, 13629–13637.
 148. Caminiti, R., Licheri, G., Piccaluga, G., and Pinna, G. (1977) X-ray Diffraction Study of a “Three-Ion” Aqueous Solution. *Chem. Phys. Letts.* **47**, 275–278.
 149. Varma, S., and Rempe, S. B. (2006) Coordination Numbers of Alkali Metal Ions in Aqueous Solutions. *Biophys. Chem.* **124**, 192–199.
 150. Licheri, G., Piccaluga, G., and Pinna, G. (1975) X-ray Diffraction Study of $CaBr_2$ Aqueous Solutions. *J. Chem. Phys.* **63**, 4412–4414.
 151. Ramos, S., Neilson, G. W., and Barnes, A. C. (2003) Anomalous X-ray Diffraction Studies of Sr^{2+} Hydration in Aqueous Solution. *J. Chem. Phys.* **118**, 5542–5546.
 152. Pfund, D. M., Darab, J. G., Fulton, J. L., and Ma, Y. (2002) An XAFS Study of Strontium Ions and Krypton in Supercritical Water. *J. Phys. Chem.* **98**, 13102–13107.
 153. Ramos, S., Barnes, A. C., Neilson, G. W., and Capitan, M. J. (2000) Anomalous X-ray Diffraction Studies of Hydration Effects in Concentrated Aqueous Electrolyte Solutions. *Chem. Phys.*

- 258, 171–180.
154. D'Angelo, P., Pavel, N., Roccatano, D., and Nolting, H. F. (1996) Multielectron Excitations at the L Edges of Barium in Aqueous Solution. Phys. Rev. B 54, 12129–12138.
 155. Linder, B., and Hoernschemeyer, D. (1967) Cavity Concept in Dielectric Theory. J. Chem. Phys. 46, 784.
 156. Wilson, M. A., Wei, C., Bjelkmar, P., Wallace, B. A., and Pohorille, A. (2011) Molecular Dynamics Simulation of the Antiamoebin Ion Channel: Linking Structure and Conductance. Biophys. J. 100, 2394–2402.